Journal of Materials Chemistry C

ROYAL SOCIETY OF CHEMISTRY

PAPER

View Article Online
View Journal | View Issue

Cite this: J. Mater. Chem. C, 2023, 11, 1579

Solution processable carbazole-benzophenone derivatives as bipolar hosts enabling high-efficiency stable green TADF organic LEDs†

Mangey Ram Nagar,[a] Krishan Kumar,[c] Dovydas Blazevicius,[b] Raminta Beresneviciute,[b] Gintare Krucaite,[b] Daiva Tavgeniene,[b] Chen Tun Hao,[a] Subrata Banik,[d] Jwo-Huei Jou *[a] and Saulius Grigalevicius *[b]

Solution-processable bipolar materials acting as hosts, soluble in common organic solvents, are key materials for thermally activated delayed fluorescence (TADF) emitters. Bipolar hosts are importantly anticipated to encourage solution-processable high-efficiency TADF organic light-emitting diodes (LEDs). Herein, we have successfully designed and synthesized solution-processable bipolar carbazole-benzophenone derivatives as host materials, *i.e.* 4,4′-di(3-phenylcarbazol-9-yl)benzophenone (**BPBCzO**) and 4,4′-di[3-[4-(carbazol-9-yl)phenyl] carbazol-9-y] benzophenone (**BCzBCzO**). These newly synthesized hosts exhibited high-triplet energies, balanced charge-transporting properties, suitable molecular orbital energy levels, good thermal stability, and good solubility, which are required to realize green TADF based organic LEDs. Initially, we fabricated two different types of TADF organic LEDs using these hosts and commercially available guest **4CzIPN** as a green dopant and compared their device characteristics. A green TADF based organic LED employing **BPBCzO** host displayed excellent performance with a maximum external quantum efficiency (EQE_{max}), current efficacy (CE_{max}), and power efficacy (PE_{max}) as high as 23.2%, 70.7 cd A^{-1}, and 55.6 l m W^{-1}, respectively. In particular, over 90% of EQE was reserved (EQE of 21.3%) at the practical luminance of 1000 cd m^{-2}, which is advantageous for display technology. At last, green OLED was also fabricated with a cross-linkable hole transport material, *i.e.* 3,6-bis(4-vinylphenyl)-9-ethylcarbazole (VPEC) and realized PE_{max} of 63.6 l m W^{-1} with EQE of 25.3%, which could be very effective for lighting and display devices. These excellent outcomes demonstrate the big potential of the carbazole-benzophenone derivatives as host materials for next-generation solution-processable display and lighting technologies.

Received 12th November 2022,
Accepted 4th January 2023

DOI: 10.1039/d2tc04820e

rsc.li/materials-c

1. Introduction

Solution processable bipolar materials have been reported as emitters and host materials in organic light emitting diodes (LEDs).[1–6] These materials exhibited a thermally activated delayed fluorescence (TADF) nature and have the capability of harvesting triplet excitons from excited triplet to singlet states by reverse intersystem crossing (RISC).[7–10] Thus, the TADF materials based organic LEDs have reached an internal quantum efficiency of nearly 100%.[11,12] Besides TADF organic LEDs, phosphorescent organic LEDs can also harvest singlet and triplet excitons because of the strong spin–orbital coupling.[13–15] However, the phosphorescent materials have been synthesized with metal complexes having difficulties such as naturally low abundant, toxic in nature, and expensive, which hampered their widespread applications.[16,17] TADF materials are designed and synthesized from pure organic units without incorporating the expensive metals.[18–20] Thus, TADF materials are more affordable in cost and comparable or superior to commercially available phosphorescent materials, which makes them promising substitutes of phosphorescent materials for the fabrication of high-efficiency organic LEDs.

High-efficiency organic LEDs can be achieved using TADF host-emitter systems, which are extensively used and reported.[21,22]

[a] Department of Materials Science and Engineering, National Tsing Hua University, Hsinchu 30013, Taiwan. E-mail: mangeyrnagar@gmail.com, andy25512@gmail.com, jjou@mx.nthu.edu.tw
[b] Department of Polymer Chemistry and Technology, Kaunas University of Technology, Radvilenu Plentas 19, LT50254, Kaunas, Lithuania. E-mail: dovydas.blazevicius@ktu.lt, raminta.beresneviciute@ktu.lt, gintare.krucaite@ktu.lt, daiva.tavgeniene@ktu.lt, saulius.grigalevicius@ktu.lt
[c] School of Basic Sciences, Department of Chemical Sciences, Indian Institutes of Technology Mandi, Himachal Pradesh, India. E-mail: krishanme906@gmail.com
[d] Department of Chemistry, School of Chemical and Biotechnology, SASTRA Deemed University, Thanjavur 613401, Tamil Nadu, India. E-mail: subratachem@gmail.com

† Electronic supplementary information (ESI) available. See DOI: https://doi.org/10.1039/d2tc04820e

TADF emitters exhibit a long triplet exciton lifetime enabling several quenching phenomena, *i.e.* triplet-polaron annihilation, singlet-triplet annihilation, triplet-triplet annihilation, and intermolecular interactions, etc, which compromise device efficiencies especially at high luminance.[23–25] In order to improve these quenching possibilities, the exhibiting high-performance TADF organic LEDs fabricated with the dispersion of TADF emitters and suitable host matrices.[26] Thus, both TADF emitter and host at the same time participate to attain high-efficiency and long-lifetime in organic LEDs.[27,28] However, compared to organic emitters, the appropriate solution processable hosts materials are hardly ever reported due to difficulties in designing host materials having important characteristics, *i.e.* high singlet-triplet energies to confine exciton in the emissive layer, suitable molecular orbital energy levels to confine charge carriers into emitters, bipolar characteristics to facile charge injection and transportation in emissive layer, easy and solubility in common solvents.[29,30] Currently, solution processable TADF organic LEDs have been attracting attention for being cost-effective, possessing a simpler design structure, and capability of being scaled up for large area displays.[30] However, most of the materials with dry process compatibility are not compatible for solution process adoption due to poor solubility and crystallization of the film upon spin casting, thus there needs to be a further investigation in synthesis of compatible small molecules. Meanwhile, dry processed host materials are continuously being designed and developed for the fabrication of high-efficiency TADF organic LEDs.[31–35] However, few reports also have established the designing, synthesis, and incorporation of solution processable hosts for organic LEDs.

Specifically, Adachi *et al.* reported a novel host material, with strong donor and acceptor units, 1,3-bis{3-[3-(9-carbazolyl)phenyl]-9-carbazolyl}benzene (CPCB), which has a high triplet energy level of 2.79 eV along with a high T_g of 165 °C. This host was doped with a green TADF emitter **4CzIPN** to fabricate organic LED and exhibited an external quantum efficiency (EQE) of 10% and a half-life of nearly 200 hours with an initial luminescence of 1000 cd m^{-2}.[36] Choi *et al.* developed two host materials with 9*H*-xanthen-9-one as an electron-accepting moiety. The bipolar hosts, namely 3-(3,5-di(9*H*-carbazol-9-yl)phenyl)-9*H*-xanthen-9-one (Xp-mCP) and 2-(3,5-di(9*H*-carbazol-9-yl)phenyl)-9*H*-xanthen-9-one (Xm-mCP) were developed and they exhibited triplet energies of 2.67 eV for Xp-mCP and of 2.82 eV for Xm-mCP. The green emitter t4CzIPN doped in Xp-mCP and Xm-mCP hosts displayed an EQE of 19.3% and 22.0% for Xp-mCP- and Xm-mCP-based green TADF-OLEDs, respectively.[37] Choi *et al.* also reported three new styrene-based copolymers (ABP91, ABP73, and ABP55) bearing strong electron-donor and electron acceptor units. Solution processed organic LED fabricated with t4CzIPN green emitter doped in the new hosts showed EQE_{max} of 21.8, 22.2, and 19.7% for ABP91, ABP73, and ABP55, respectively.[1] Zhao *et al.* reported on a series of novel polymer hosts, consisting of tetra-substituted carbazole units. These hosts exhibit triplet energies in the range of 2.23–2.25 eV. Among these polymer hosts, one devices with the known 4CzCNPy as the green TADF emitter displayed EQE_{max} of 5.7%.[38] Shao *et al.* developed a series of polymeric bipolar hosts having carbazole and aryl phosphine oxide as electron donor and acceptor units, respectively, which provides tuneable triplet energies in the range of 2.20–3.01 eVs.[39] These results support the awareness that solution-processable hosts for high-efficiency TADF organic LED fabrications have very limited availability and the performance of devices using these materials is meaningfully poorer to that of devices fabricated *via* the vacuum thermal evaporation process. Thus, potential small molecules that attribute the key characteristics required for working as host persist as an imperative requirement for the elevation of solution-processable TADF OLEDs.

To address these issues, we developed and demonstrated two carbazole–benzophenone derivatives (**BPBCzO** and **BCzBCzO**) that consist, respectively, of phenyl carbazole or carbazolyl-phenyl carbazole as the electron donor and benzophenone as an electron acceptor. In this design strategy, we have chosen the substituted carbazoles because of their facile charge injection and transport capabilities. These donor units have also influenced the triplet energies of the novel hosts, which resulted in 2.7 and 2.6 eV, respectively, which make them applicable for green and blue TADF organic LEDs. Moreover, these materials exhibited high thermal stability in terms of high decomposition temperature and glass transition temperature (T_g). The decomposition temperatures (T_d) for **BPBCzO** and **BCzBCzO** were 277 and 371 °C, and T_g were of 92 and 187 °C, respectively. The derivatives have also excellent solubility in organic solvents (*e.g.*, tetrahydrofuran, toluene, chloroform, and chlorobenzene), which certify their processability in solution process methods. Therefore, the solution processed organic LEDs were fabricated with these new solution processable hosts and commercially available green TADF emitter **4CzIPN**. The **BPBCzO** and **BCzBCzO** based green TADF organic LEDs exhibited EQE_{max} of 23.2 and 15.3%, PE_{max} of 55.6 and 46.2 l m W^{-1}, CE_{max} of 70.7 and 49.2 cd A^{-1}, and lifetime (at 10 000 cd m^{-2}) of 2.2 and 1.5 hr, respectively. On comparing these devices, we found that the phenyl substituted carbazole-benzophenone (**BPBCzO**) based device displayed higher performance as compared with other host-based device.

In addition, we incorporated crosslinkable hole transporting material in similar organic LED design to achieve higher efficiency as well as lifetime. Therefore, cross-linkable hole transporting material: 3,6-bis(4-vinylphenyl)-9-ethylcarbazole (VPEC) based green TADF organic LED (fabricated with **BPBCzO** host) displayed an EQE_{max} of 25.3%, PE_{max} of 63.6 l m W^{-1}, CE_{max} of 81.0 cd A^{-1}, and lifetime (at 10 000 cd m^{-2}) of 3.2 h. These results also confirm that this work will make a significant contribution through the introduction of a variety of solution processable materials that function as hosts for the development of proficient solution-process-able TADF OLEDs.

2. Results and discussion

2.1. Synthesis and characterization

The objective materials **BPBCzO** and **BCzBCzO** were synthesized following a three-step synthesis process as shown in Scheme 1.

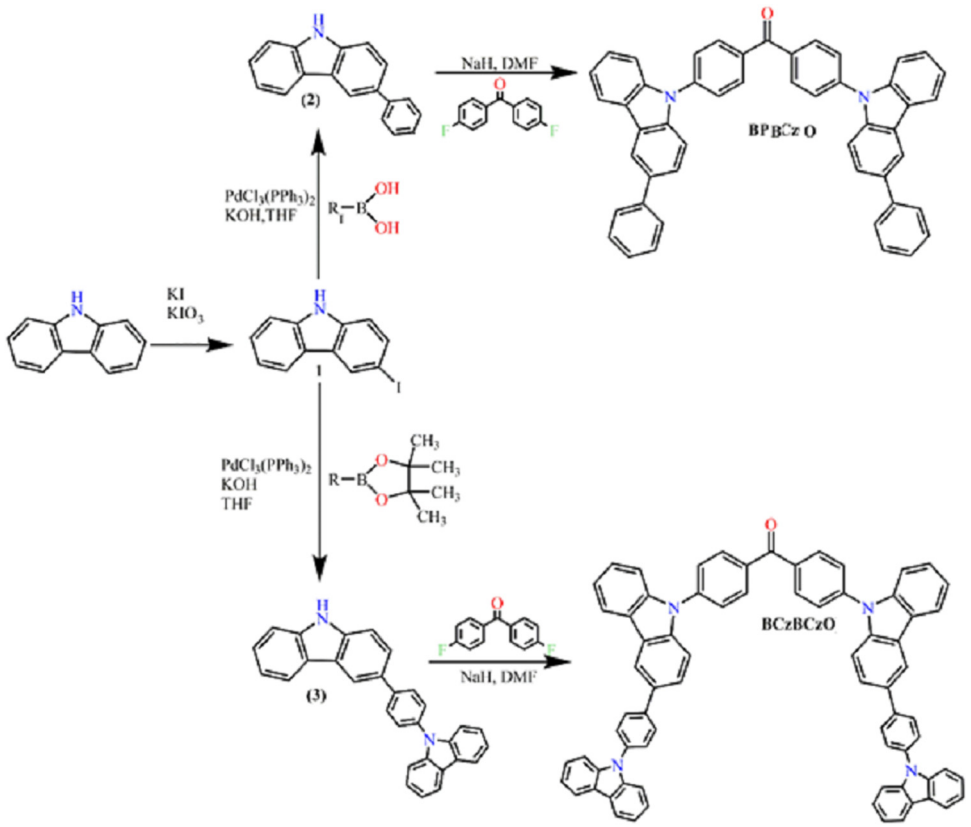

Scheme 1 Synthetic pathway of materials **BPBCzO** and **BCzBCzO**.

3-Iodo-9*H*-carbazole (**1**) was firstly obtained by a procedure of Tucker.[40] Intermediate carbazole based derivatives **2** and **3** were then prepared by Suzuki reaction, when the 3-iodo-9*H*-carbazole (**1**) reacts with an excess of corresponding boronic acid or boronic acid pinacol ester under basic conditions. Further, the reaction was catalysed by the palladium catalyst. Finally, the objective compounds **BPBCzO** and **BCzBCzO** were received by nucleophilic *N*-substitution reaction of the mentioned carbazole based compounds **2** or **3** with 4,4′-difluorobenzophenone using basic conditions of K_2CO_3. The synthesized derivatives were identified by mass spectrometry, ^{1}H and ^{13}C NMR spectroscopy. The data were found to be in good agreement with the proposed structures. The derivatives were soluble in common organic solvents at room temperature. Transparent thin films of these materials could be prepared by spin coating from their solutions.

2.2. Molecular structure analysis

To understand the electronic states of the newly developed compounds, theoretical calculations have been done by Gaussian09 software at the level of B3LYP (hybrid functional) and 6-311G(d,p) basis set. The optimized geometries of all the compounds exhibit a significantly twisted structure due to the two phenyl rings of benzophenone being located asymmetrically on each side of the donor moieties. All the molecules possess donor–acceptor characteristics as the almost complete separation of the HOMO and LUMO at the donor and acceptor (benzophenone) moieties are observed (Fig. 1).

The theoretical HOMO energy levels were calculated to be −5.72 eV and −5.63 eV for **BPBCzO**, and **BCzBCzO**, respectively. Similarly, the LUMO energy levels were calculated to be −2.29 eV and −2.31 eV for **BPBCzO** and **BCzBCzO**, respectively (Table 1). The frontier molecular orbital distribution confirmed that the synthesized molecules are having donor–acceptor–donor architecture in their chemical structures. Furthermore, the angle between carbazole and benzophenone was measured from their optimized geometries. It was observed that the carbazole based units are tilted at an angle of ∼58–59° with respect to the benzophenone unit, which concluded that the effective conjugation within the units is not uniform, by which both the units possess the overall twisted geometry in the molecules. As the designed molecules possess suitable frontier molecular orbitals (FMOs) and donor–acceptor–donor characteristics with twisted geometries, these molecules could be suitable for the optoelectronic device applications. As the singlet and triplet energy levels of the host materials are very crucial for the device performance, the S_1 and T_1 levels of the compounds were calculated from time-dependent DFT (TD-DFT) within Tamm-Dancoff approximation (TDA), by choosing the same solvent system (DCM) and the same basis set. The excited state energies were vertical calculated at the optimized geometries of the ground states for each molecule. The calculated singlet energy values for **BPBCzO** and **BCzBCzO**

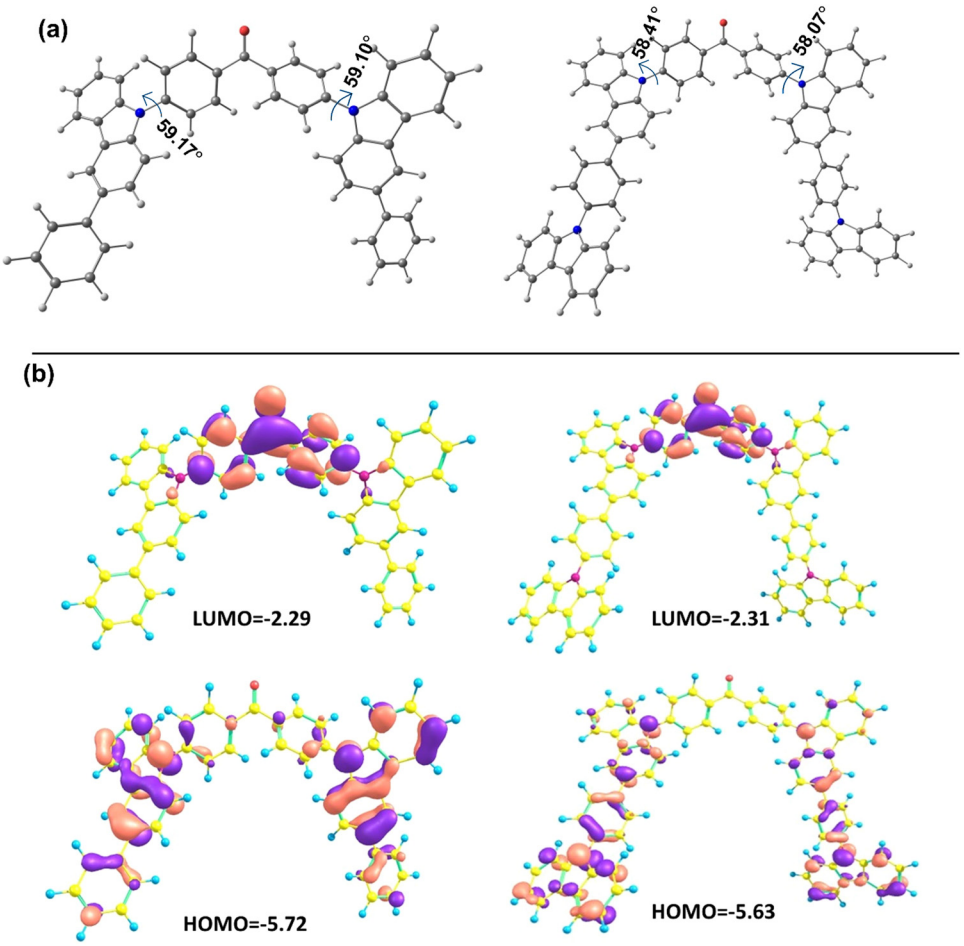

Fig. 1 Theoretical studies of newly synthesized derivatives. (a) The angle between donor–acceptor units and (b) HOMO/LUMO distributions of the **BPBCzO** and **BCzBCzO** molecules.

Table 1 Photo-physical, thermal, theoretical, and electrochemical characteristics of **BPBCzO** and **BCzBCzO** materials

Comp.	λ_{abs} [a] (nm)	λ_{PL} [b] (nm)	λ_{PL} [c] (nm)	T_m [d] (°C)	T_g [e] (°C)	T_d [f] (°C)	HOMO/LUMO [g] (−eV)	HOMO/LUMO [h] (−eV)	E_s/E_t [i] (−eV)	E_s/E_t [j] (−eV)	E_g [k] (eV)
BPBCzO	353	434	515	123	92	277	5.72/2.29	6.15/2.63	2.97/2.78	2.83/2.64	4.1
BCzBCzO	345	433	534	366	187	371	5.63/2.31	6.05/2.45	2.95/2.78	2.77/2.60	4.0

[a] Absorbance peaks. [b] Photoluminescence (PL) spectra peak measured at room temperature. [c] PL spectra peak measured at 77 K. [d] Melting temperature. [e] Glass transition temperature. [f] Decomposition temperature. [g] HOMO and LUMO calculated by DFT. [h] HOMO and LUMO obtained by cyclic voltammetry (CV) technique. [i] Calculated triplet (E_t) and singlet (E_s) energies by DFT. [j] Measured triplet (E_t) and singlet (E_s) energies. [k] Optical band-gap (E_g) energy.

are 2.97 eV and 2.95 eV, respectively. Similarly, the triplet energy values for **BPBCzO** and **BCzBCzO** are 2.78 eV and 2.78 eV, respectively. The higher wavelength peaks observed in the TD spectrums (*i.e.* 417 nm and 420 nm for **BPBCzO** and **BCzBCzO**, respectively) are due to the charge transfer from donor to acceptor moieties (Fig. S5 and S6 in ESI†). The TD-DFT analysis of S0 → S1 transitions of both the molecules corresponding to their transition energy, MO involved, and oscillator strengths have been listed in the Table S1 (ESI†). Thus, the theoretical simulation results of these molecules ensure that these molecules could be promising hosts for OLED devices.

2.3. Thermal and morphological properties

The behaviour under heating of the synthesized materials **BPBCzO** and **BCzBCzO** was studied by DSC and TGA under a nitrogen atmosphere. It was established that the objective compounds demonstrate high thermal stability. The temperature of 5% weight loss for derivatives **BPBCzO** and **BCzBCzO** was 277 °C and 371 °C respectively (Table 1), as confirmed by TGA with a heating rate of 10 °C min^{-1} and could be seen in Fig. S14 and S15 (ESI†). The compounds **BPBCzO** and **BCzBCzO** were obtained as crystalline materials after synthesis as confirmed by DSC, however, they could be easily converted to amorphous materials by cooling the melted sample. The DSC

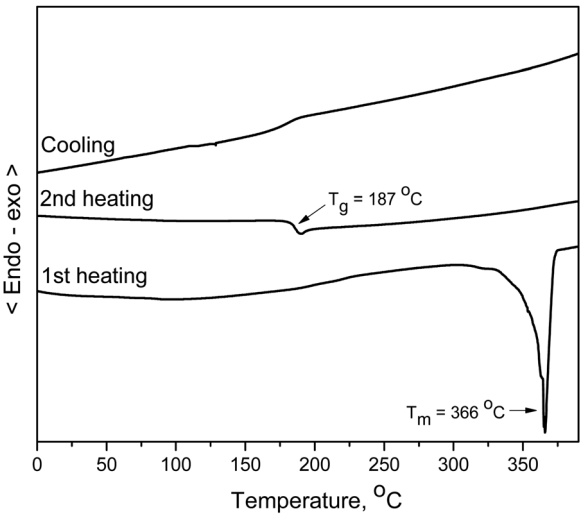

Fig. 2 DSC curves of compound **BCzBCzO**. Heating rate: 10 °C min^{-1}.

measurement of material **BCzBCzO** is demonstrated in Fig. 2 as an example. During the first heating, an endothermic melting peak was observed at 366 °C for the melting temperature. When the melted sample was cooled down, the mentioned derivative **BCzBCzO** formed an amorphous material with a glass transition temperature of 187 °C as could be seen from the second heating scan. During the first heating of the DSC experiment, an endothermic melting peak was also observed at about 123 °C for crystalline material **BPBCzO**. When the melt was cooled down, the derivative formed an amorphous material with a glass transition temperature (T_g) of about 92 °C.

To investigate surface morphologies and film-forming abilities of thin-films prepared by mixing the hosts **BPBCzO** and **BCzBCzO** with guest **4CzIPN**, atomic force microscopy (AFM) was utilized, as shown in Fig. 3. In this aspect, solutions of the hosts or blended solution of 5 wt% of **4CzIPN** with the hosts in toluene were spin-coated on PEDOT:PSS thin-film or layer of VPEC deposited on a glass substrate. As shown in the figure, all the prepared thin-films have homogenous and smooth morphologies having very small average roughness values of 0.52 and 0.68 nm for **BPBCzO** and **BCzBCzO**, respectively. The homogenous and smooth films having small roughness would facilitate the charge transport at the interface of HTL/EML and EML/ETL, which is one of the key requirements for achieving high efficiencies in OLEDs. It can also be observed that all the films do not display phase separation and particle aggregation, which is favourable for enhancing OLED performance. It is observed that the **BPBCzO** exhibits a lower average roughness (0.53 nm) as compared with **BCzBCzO** (0.68 nm). It is also seen that the doping of **4CzIPN** into **BPBCzO** and **BCzBCzO** reduced average roughness to 0.23 and 0.43 nm, respectively. On the other hand, by using cross-linked layer of HTM VPEC the roughness was further reduced to 0.23 These outcomes advocate the idea that the blending of a new host and dopant is very preferable for the fabrication of cost-effective solution-processable OLEDs.

2.4. Optical and photophysical properties

To determine the photophysical properties of these new hosts, *i.e.* **BPBCzO** and **BCzBCzO**, ultra-violet-visible (UV-Vis) absorption and photoluminescence (PL) studies were performed in toluene solution, as shown in Fig. 4. These hosts exhibit absorption features with peaks positioned at 353 and 345 nm in solution. Furthermore, we did not observe any red-shifted

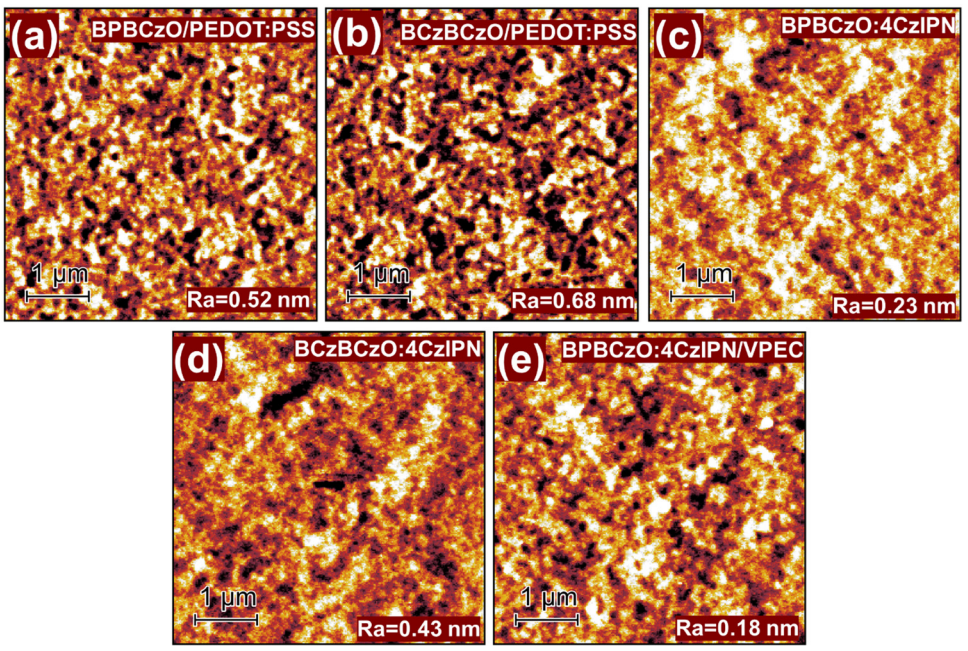

Fig. 3 Surface morphologies and average roughness of (a and b) **BPBCzO** and **BCzBCzO** thin-films prepared on PEDOT:PSS, respectively, (c and d) **BPBCzO**:**4CzIPN** and **BCzBCzO**:**4CzIPN** prepared on PEDOT:PSS, respectively, (e) **BPBCzO**:**4CzIPN** thin-film prepared on cross-linked HTM VPEC.

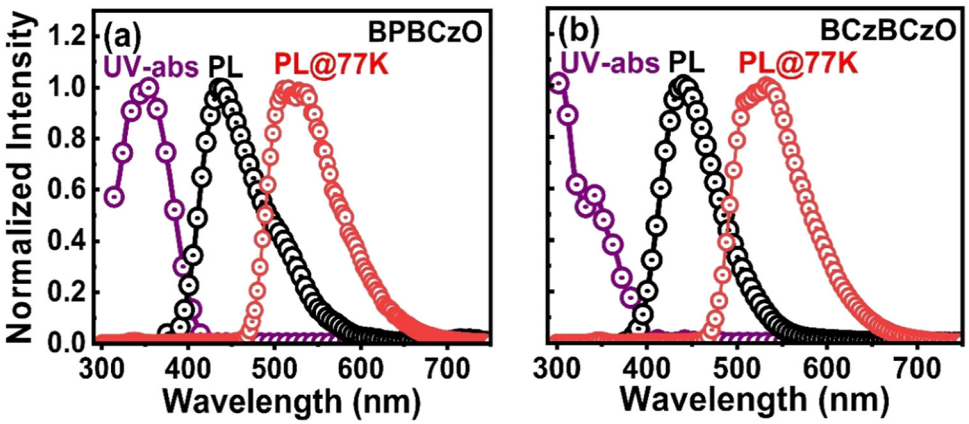

Fig. 4 UV-vis absorption and photoluminescence (PL) spectra of (a) **BPBCzO** and (b) **BCzBCzO** in toluene. Low-temperature PL spectra (LTPL) measured in toluene at 77 K are also included.

absorption peaks in the spectra, which indicates that intramolecular energy transfer between donor and acceptor units does not exist. The optical band gaps were calculated from the absorption spectra to be 300 nm and 310 nm for **BPBCzO** and **BCzBCzO**, as listed in Table 1. Further, the NTO (natural transition orbital) diagrams for different transitions for **BPBCzO** and **BCzBCzO** are given in Fig. S7 (ESI†). The photoluminescence (PL) spectra of the hosts in toluene solvent exhibited emission with peaks at 434 and 433 nm, respectively, as shown in Fig. 4.

The triplet energies of **BPBCzO** and **BCzBCzO** were estimated from the first triplet emission peak of the phosphorescence spectra measured in cryogenic medium (liquid N_2) at 77 K as shown in Fig. 4. **BPBCzO** and **BCzBCzO** showed triplet-energies of 2.64 eV and 2.60 eV, respectively. Thus, the resulting triplet energies are high enough for efficient energy transfer and to avoid a back-energy transfer from the **4CzIPN** green emitter, indicating that these materials can be used as host materials.

2.5. Electrochemical properties

Electrochemical properties were investigated in the solution phase of **BPBCzO** and **BCzBCzO** in DCM solvent utilizing cyclic voltammetry (CV) (Fig. S4, ESI†). As displayed in the Figure, all newly synthesized host materials exhibit a quasi-reversible oxidation potential ($E^{ox}_{1/2}$) peak, which may be originated from different electron-donating units, *i.e.* *X* and *Z*. From the CV curves, the oxidation potentials of **BPBCzO** and **BCzBCzO** were estimated to be +1.35 and +1.25 V, respectively. Accordingly, the highest occupied molecular orbital (HOMO) energy levels of these materials were calculated to be 6.15 and 6.05 eV, respectively, by substituting $E^{ox}_{1/2}$ in the following equation HOMO = $-(EE^{ox}_{1/2}$ +4.8). The lowest unoccupied molecular orbitals (LUMO) energy levels of these materials, which were confirmed by substituting the HOMO energy-levels and optical bandgap E^{opt}_g in the following equation LUMO (eV) = HOMO (eV) + E^{opt}_g (eV), and calculated to be −2.63 eV and −2.45 eV. **BPBCzO** and **BCzBCzO** showed almost similar HOMO levels. **BCzBCzO** displayed shallower LUMO energy levels as compared with **BPBCzO**. The HOMO and LUMO energies are well aligned to those of common charge-transporting materials and emitter materials used in OLEDs, which are conductive for facile charge injection and transportations.

2.6. Energy transfer process

To confirm the effective energy transfer between the hosts and guest, the overlapping areas between the PL spectra of hosts and the UV-vis spectrum of the guests were estimated as shown in Fig. 5. The large overlapping area indicates that the energy transfer from host to guest is effective and efficient. We observed that **BPBCzO** exhibited a larger overlapping area as compared with **BCzBCzO**, as shown in the Fig. 5(a and b).

Lower overlapping area between the PL peak of **BCzBCzO** and the absorption peak of **4CzIPN** suggests smaller energy transfer from **BCzBCzO** to **4CzIPN** guest material. The overlapping area between **BPBCzO** emission peak and **4CzIPN** absorption peak is slightly higher, as shown in Fig. 5(a), which would trigger the higher energy emission of the guest, leading to higher device efficiency. Furthermore, the energy-transfer routes are shown in Fig. S3 (ESI†). We observed that the hosts **BPBCzO** and **BCzBCzO** possess singlet energies of 2.83 and 2.77 eV, which are higher than that of the green TADF emitter **4CzIPN** (2.4 eV). This would permit hosts to empower a host-to-guest energy transfer and exciton confinement on the emitters, ensuing in high device efficiency.

2.7. Charge-transport properties

To investigate the relationship between chemical structures and charge-transporting capabilities of **BPBCzO** and **BCzBCzO**, single charge carriers devices, *i.e.* hole-only devices (HODs) and electron-only devices (EODs) having following device configurations: [ITO (150 nm)/PEDOT:PSS (35 nm)/TAPC (10 nm)/**BPBCzO** or **BCzBCzO** (20 nm)/TAPC (10 nm)/Al (100 nm)] (HODs) and [ITO (150 nm)/TPBi (20 nm)/**BPBCzO** or **BCzBCzO** (20 nm)/TPBi (40 nm)/LiF (0.8 nm)/Al (100 nm)] (EODs) were fabricated, as shown in Fig. S8 (ESI†). The organic interlayers, such as PEDOT:PSS and TAPC, were incorporated in HODs to facilitate hole-injection from the ITO to newly synthesized host

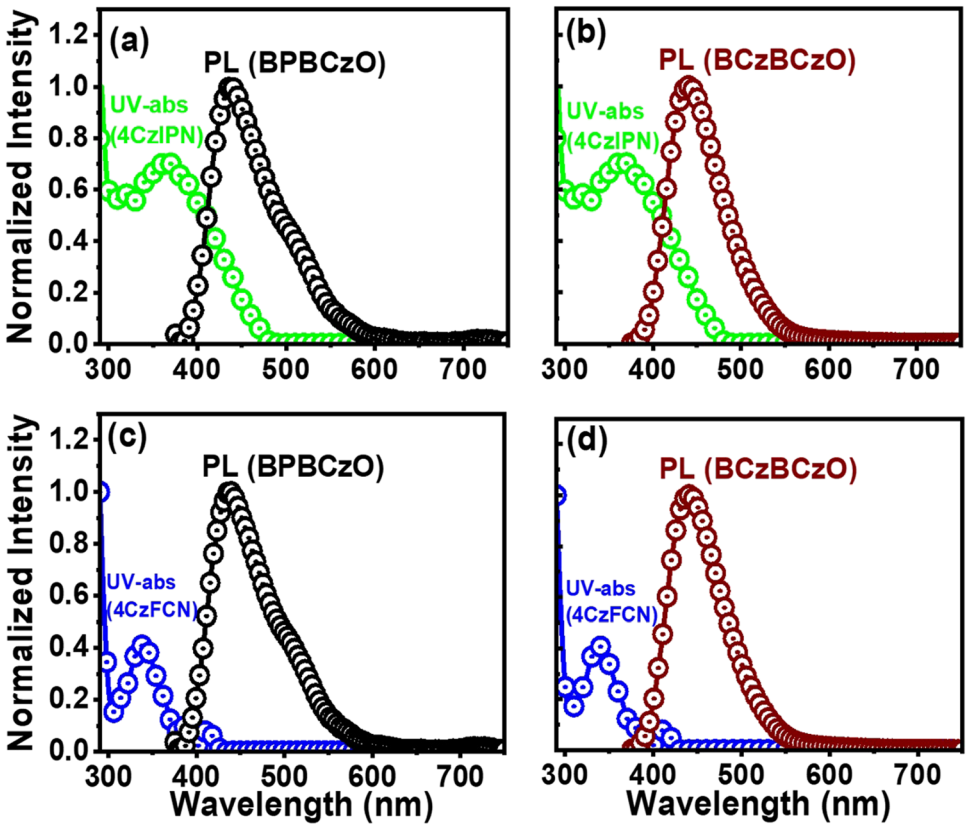

Fig. 5 Overlapping of UV-vis spectrum of green TADF emitter and PL of **BPBCzO** (a) and **BCzBCzO** (b).

materials, whereas TPBi and LiF in EODs enable electron-injection from the cathode, *i.e.* Al, to host materials. The current density–voltage characteristics of the HODs and EODs are shown in Fig. S9 (ESI†). The newly synthesized host materials exhibit significant hole and electron current densities due to substituted carbazole donor and benzophenone acceptor units. **BPBCzO** exhibited higher hole current density as compared to other presented host, indicating that **BPBCzO** possesses better hole transport characteristics. As observed, **BPBCzO** demonstrated higher current density in EOD, indicating that the benzophenone unit influenced the electron-transport ability of this material. We also observed that both the materials have shown similar hole and electron current densities at the same applied voltage, which implies that these materials exhibit balanced charge injection and transport properties. After careful investigation, we observed that the **BPBCzO** host displayed a balance of charge carriers, confirming the superior host properties. Theoretically we observed that these materials exhibit well-separated HOMO and LUMO energy levels and high charge current densities in single carrier devices, depicting their bipolar nature. The bipolar nature of the host materials enhances the charge injection and recombination zone, reducing charge accumulation and exciton quenching, and leading to superior device performance at high luminance. Therefore, by designing and synthesizing the bipolar host materials, we were able to achieve the key requirements for solution-processed organic LEDs which can improve the devices performance.

2.8. Electroluminescent (EL) properties

2.8.1 TADF Green organic LEDs. The superior characteristics, *i.e.* appropriate high triplet energy (E_T), suitable bandgap energy levels, good thermal stability, and admirable solubility in common organic solvents of these derivatives, motivated us to explore their capability as hosts for the application in solution-processed TADF based organic LEDs. The green TADF organic LEDs consisted following device configurations: ITO (125 nm)/PEDOT:PSS (35 nm)/**BPBCzO** or **BCzBCzO**: X wt% **4CzIPN** (20 nm)/PO-T2T (10 nm)/TPBi (30 nm)/LiF (1 nm)/Al (200 nm). The molecular structures of the utilized materials in the device and their energy levels are shown in Fig. S1 and S2 of ESI.† The EL properties of solution processed TADF organic LEDs with different hosts **BPBCzO** or **BCzBCzO** doped with different concentrations of guest are displayed in Fig. S10 and S11 (ESI†), respectively, and summarized in Table S1 (ESI†). The effects of doping concentration on EL spectra of **BPBCzO** and **BCzBCzO** based green TADF organic LEDs are shown in Fig. S12(a) and (b) (ESI†), respectively. The EL spectra (Fig. S12, ESI†) display that both devices exhibited green emissions with the peak wavelength at 520 nm, which is comparable to the PL spectrum of the **4CzIPN**.[41,42]

The EL characteristics of the devices are demonstrated in Fig. 6, and their corresponding values are summarized in Table 2. Luminance–voltage curves indicate that the **BPBCzO** based device emitted higher brightness as compared to **BCzBCzO** based device at the same voltage (7.0 V). **BPBCzO**

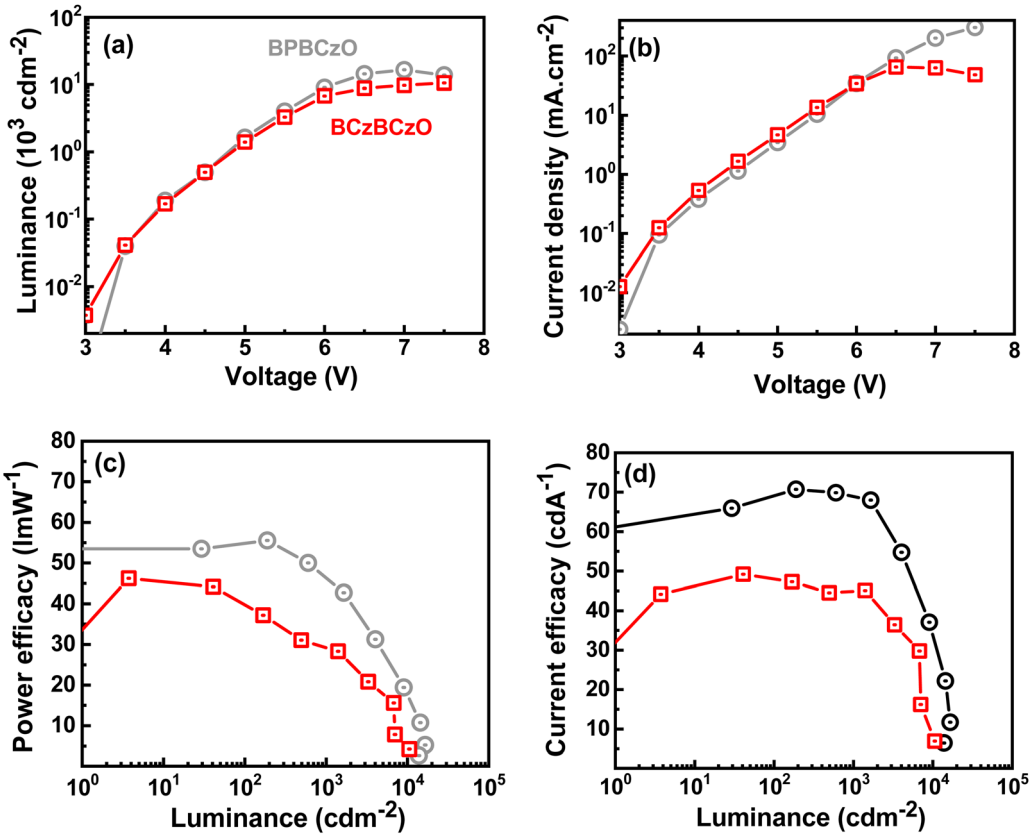

Fig. 6 TADF based organic LEDs characteristics: (a) luminance, (b) current–density, (c) power efficacy, and (d) current efficacy. The emitting layers are fabricated from **BPBCzO** (grey line with circle) or **BCzBCzO** (red line with square) doped with **4CzIPN**.

based device displayed a turn-on voltage (V_{on}) of 3.0 V, which is higher than that of **BCzBCzO** based device (2.7 V), as shown in Table 1 and Fig. 6(b). Lower turn-on voltage indicates that more efficient charge injection has happened from the charge transport layers (HTL and ETL) to the emissive layer because of the low energy barrier. **BCzBCzO** based device displayed higher current density as compared to **BPBCzO** based device. Higher current density may be attributed to the higher roughness of **BCzBCzO** based EML and unbalanced charge-injection into the device (as shown in Fig. S6(b), ESI†). The devices having **BPBCzO:4CzIPN** and **BCzBCzO:4CzIPN** obtained a maximum EQE/maximum CE/maximum PEs as high as 23.2%/70.7 cd A^{-1}/55.6 l m W^{-1} and 15.3%/49.2 cd A^{-1}/46.2 l m W^{-1}, respectively, as shown in Table 1 and Fig. 6(c and d).

Among these outcomes, **BPBCzO** based device displayed the best performance with a maximum PE, CE and EQE of 55.6 l m W^{-1}, 70.7 cd A^{-1} and 23.2%, respectively, along with a maximum brightness of 16 500 cd m^{-2}. Remarkably, **BPBCzO** based device displayed a roll-up character with EQE at 1000 cd m^{-2} reached up to 21.3% from 21.0% EQE at 100 cd m^{-2}. The reason for the roll-up character can be explained as follows: balanced charge injection and transport, smooth surface roughness, and reduced exciton quenching at higher brightness.

Additionally, it is observed that **BPBCzO** based single carrier devices (as shown in Fig. S6, ESI†) displayed a more balanced hole and electron transport as compared with **BCzBCzO**, which leads to the highest performance and efficiency roll-up nature between these two host materials. The lower performance of **BCzBCzO** based device can be attributed to the low PLQY (55%) of **4CzIPN** doped **BCzBCzO** layer and slightly lower triplet energy of 2.60 eV of the host, which may permit back energy transfer from guest to host and thus leading to reduced performance. The electroluminescence (EL) spectra (as shown in Fig. S12, ESI†) show that the devices fabricated with **BPBCzO** and **BCzBCzO** exhibit green emissions with the wavelength placed between 520 and 524 nm, which is equal to the reported

Table 2 EL properties of **BPBCzO** and **BCzBCzO** hosts based green TADF organic LEDs

			Power efficacy (l m W^{-1})			Current efficacy (cd A^{-1})			External quantum efficiency (%)				
Hosts	HTL	V_{on} (V)	Max.	@100 cd m^{-2}	@1000 cd m^{-2}	Max.	@100 cd m^{-2}	@1000 cd m^{-2}	Max.	@100 cd m^{-2}	@1000 cd m^{-2}	CIE$_{xy}$@100 cd m^{-2}	L_{max} cd m^{-2}
BPBCzO	—	3.0	55.6	54.3	43.1	70.7	64.1	64.8	23.2	21.0	21.3	(0.28,0.57)	16 500
	VPEC	2.9	63.6	62.0	49.5	81.0	72.3	73.4	25.3	22.6	23.0	(0.29,0.58)	18 900
BCzBCzO	—	2.7	46.2	40.9	29.5	49.2	48.3	44.8	15.3	15.0	14.0	(0.28,0.57)	10 540

PL spectrum of **4CzIPN**,[41] confirming that the recombination happens within the **4CzIPN**.

2.8.2 Incorporation of cross-linkable HTL. We incorporated cross-linkable HTL of 3,6-bis(4-vinylphenyl)-9-ethylcarbazole (VPEC)[43] into the **BPBCzO** based OLED to achieve improved charge injection and balance for improving a high-efficiency and long lifetime of the best performing device. The effects of VPEC layer on EL properties such as current–density, luminance, power efficacy, current efficacy, and EL spectra of the devices fabricated are shown in Fig. 7 and their EL characteristics data are summarized in Table 2.

In order to investigate the effects of VPEC layer, current–density and luminance were measured at varying voltages, as shown in Fig. 7(a) and (b). For the green TADF device, the increased current–density and luminance in the device is displayed with VPEC, which indicates that the incorporation of VPEC facilitates improved hole injection into EML due to its appropriate HOMO level (5.3 eV). Among these TADF devices, VPEC based device showed better performance than that of device without VPEC. The maximum PE, CE, and EQE were changed from 55.6 to 63.6 l m W^{-1}, from 70.7 to 81.0 cd A^{-1}, and from 23.2 to 25.3% as VPEC employed in the device, as shown in Fig. 7(c) and (d) and Table 2. This increment in the performance may be attributed to the following key factors: (i) reduced exciton quench by the PEDOT:PSS, (ii) good hole transport ability, (iii) reduced hole injection barrier till 0.7 eV from 1.0 eV, which facilitates injection and transport of holes, (iv) prevention of triplet energy transfer from emitter **4CzIPN** to VPEC due to its high triplet-energy.

2.8.3 Lifetime measurement. At last, the operational stability of the fabricated devices was assessed. Initially, operational half lifetime (LT_{50}) was measured at initial brightness (L_0) of 10 000 cd m^{-2} for green TADF devices fabricated with **BPBCzO** or **BCzBCzO** host, as shown in Fig. 8(a). A remarkable enhancement in device operational stability is displayed for **BPBCzO** based device, which resulted in a LT_{50} (the lifetime of luminance decay up to 50% of its initial brightness) of 2.2 h. However, a rapid luminance decay with increasing operational time is observed for **BCzBCzO** based device. **BCzBCzO** based device exhibited a LT_{50} of 1.5 hr at the same initial brightness. Moreover, the estimated LT_{50} of **BPBCzO** based device is 110 and 5526 h at 1000 and 100 cd m^{-2}, respectively. In contrast, LT_{50} of **BCzBCzO** based device is estimated 75 and 3768 h at 1000 and 100 cd m^{-2}, respectively. Enhancement in operational lifetime may be attributed to balanced charge carrier injection and transport in **BPBCzO** host, higher stability of **BPBCzO**, smooth surface roughness of **BPBCzO** based emissive layer, and low-current operation of **BPBCzO** based devices.[44,45] Operational lifetime is assessed for green TADF device fabricated with and without crosslinkable HTM VPEC as shown in Fig. 8(b). Remarkably, the green TADF device fabricated with VPEC exhibited higher operational device stability as compared

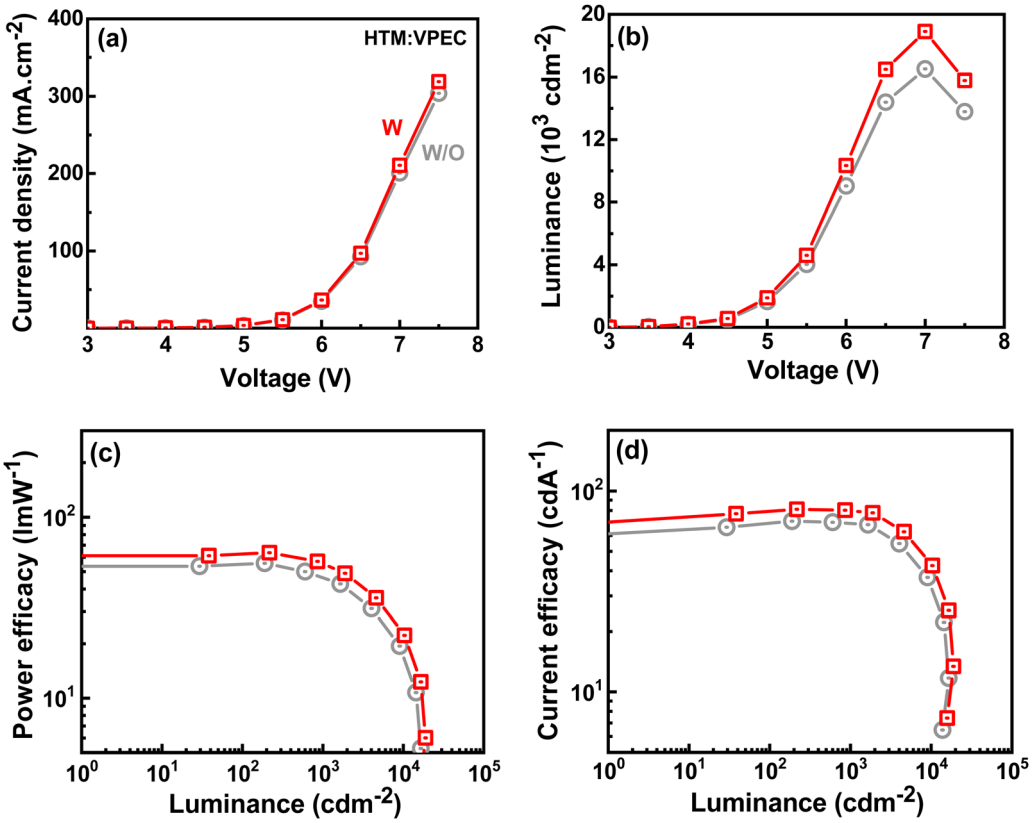

Fig. 7 EL characteristics: (a) current–density, (b) luminance, (c) power efficacy, and (d) current efficacy of **BPBCzO** based TADF organic LEDs fabricated with (red line) and without (grey line) crosslinkable VPEC.

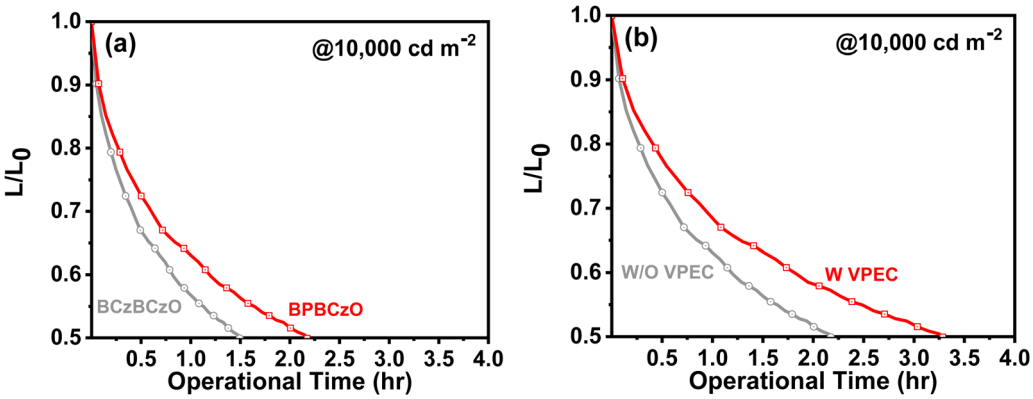

Fig. 8 Operational half lifetime (LT_{50}) of green TADF devices fabricated (a) with **BPBCzO** or **BCzBCzO** and (b) with and without crosslinkable HTM VPEC in **BPBCzO** host-based device.

to without VPEC based device. TADF device fabricated with VPEC possessed a LT_{50} of 3.2 h at L_0 of 10 000 cd m^{-2}, which is higher than that of the device fabricated without VPEC (2.2 h). Additionally, this device displayed estimated LT_{50} of 160 and 8038 h at L_0 of 1000 and 100 cd m^{-2}, respectively. Our results show that the molecular structure reported in this research may provide a path to research scholars for developing new molecules and devices, which may greatly improve efficiency along with good device stability.

3. Conclusions

In conclusion, substituted carbazole-benzophenone (donor–acceptor–donor type) based host materials, *i.e.* **BPBCzO** and **BCzBCzO**, are designed and facilely synthesized. These resulting materials displayed a bipolar transport characteristic, high triplet-energy, suitable frontier molecular orbital energy levels, and good solubility in common organic solvents. Consequently, **BPBCzO** and **BCzBCzO** were successfully incorporated with **4CzIPN** for the fabrication of solution-processed green TADF organic LEDs. Remarkably, green TADF device employing **BPBCzO** host material and **4CzIPN** guest material displays a maximum power efficacy (PE_{max}), current efficacy (CE_{max}), external quantum efficiency (EQE_{max}), and luminance (L_{max}) of 55.6 l m W^{-1}, 70.7 cd A^{-1}, 23.2%, and 16 500 cd m^{-2}, respectively. Moreover, this device exhibited an operational half lifetime of 110 h at initial brightness of 1000 cd m^{-2} and estimated 5526 h at initial brightness of 100 cd m^{-2}. Additionally, cross-linkable hole transport material **VPEC** was successfully incorporated into green TADF organic LEDs to achieve stable solution processed organic LED with high-efficiency. Corresponding device displayed a PE_{max} of 63.6 l m W^{-1}, CE_{max} of 81.0 cd A^{-1}, EQE_{max} of 25.3%, and L_{max} of 18 900 cd m^{-2}. Moreover, both type of devices displayed a roll-up character. These devices are among highly efficient solution-processable TADF organic LEDs. These noteworthy performances displayed by the TADF devices with substituted carbazole-benzophenone derivatives confirmed the potential of such host materials design strategy and provides a path for the materials design and their application in solution processable TADF organic LEDs.

4. Experiments

4.1. Materials

In this study, the primary chemicals for synthesizing the carbazole–benzophenone derivatives host materials were purchased from Sigma-Aldrich and used as received. The primary chemicals are carbazole, phenylboronic acid, naphthalene-1-boronic acid, 4-(trifluoromethyl)phenylboronic acid, 9*H*-carbazole-9-(4-phenyl) boronic acid pinacol ester, 4,4′-difluorobenzophenone, bis(triphenylphosphine)palladium(II) dichloride, KOH, NaH, KI, KIO_3, Na_2SO_4, dimethylformamide, chloroform, and tetrahydrofuran. The organic materials for thermally activated delayed fluorescence-based organic light-emitting diode fabrication, *i.e.* 2,4,5,6-tetra(9*H*-carbazol-9-yl)isophthalonitrile (**4CzIPN**) as TADF green emitter, 1,3,5-tris(*N*-phenyl benzimidazol-2-yl)benzene (TPBi) as an electron-transport material, were bought from Shine Materials Technology Co. Ltd, Taiwan. Moreover, inorganic materials, *i.e.* lithium fluoride (LiF) and aluminium ingots (Al) were incorporated as cathode material, which was also bought from Shine Materials Technology Co. Ltd, Taiwan.

4.2. Synthesis

4.2.1 3-Iodocarbazole (1). Was obtained by Tucker iodation reaction.[40] 3-Phenyl-9*H*-carbazole (2). 1.00 g (3.12 mmol) of 3-iodo-9*H*-carbazole, 0.62 g (5.09 mmol) of phenylboronic acid, 0.043 g (0.06 mmol) of $PdCl_2(PPh_3)_2$ and 0.96 g (17.11 mmol) of powdered potassium hydroxide were stirred in 10 ml of THF containing degassed water (1.5 ml) at reflux under nitrogen for 4 h. After TLC control the reaction mixture was cooled and quenched by the addition of ice water. The product was extracted by chloroform. The combined extract was dried over anhydrous Na_2SO_4. The crude product was purified by silica gel column chromatography using the mixture of ethylacetate and hexane (vol. ratio 1 : 10) as an eluent. Yield: 0.80 g (83%) of yellow material. MS (APCI+, 20 V): 244.30 ([M + H], 100%).

^{1}H NMR (400 MHz, $CDCl_3$, δ, ppm): 8.47 (s, 1H, Ar), 8.04 (d, 4H, J = 7.6Hz, Ar), 7.69 (d, 2H, J = 8.4Hz, Ar), 7.45 (s, 1H, Ar), 7.47-7.23 (m, 5H, Ar). ^{13}C NMR (400 MHz, $CDCl_3$, δ, ppm): 139.48, 139.46, 138.59, 138.56, 134.12, 134.07, 129.29, 129.25, 126.60, 122.11, 120.49, 119.97, 112.63, 112.60, 110.81, 110.75.

4.2.2 3-[(4-(Carbazol-9-yl)phenyl)-9*H*-carbazole] (3). 2.50 g (8.53 mmol) of 3-iodo-9*H*-carbazole, 4.73 g (12.81 mmol) of 9*H*-carbazole-9-(4-phenyl) boronic acid pinacol ester, 0.119 g (0.17 mmol) of $PdCl_2(PPh_3)_2$ and 0.96 g (17.11 mmol) of powdered potassium hydroxide were stirred in 25 ml of THF containing degassed water (3.75 ml) at reflux under nitrogen for 4 h. After TLC control the reaction mixture was cooled and quenched by the addition of ice water. The product was extracted by chloroform. The combined extract was dried over anhydrous Na_2SO_4. The crude product was purified by silica gel column chromatography using the mixture of ethyl acetate and hexane (vol. ratio 1 : 7) as an eluent. Yield: 2.22 (45.6%) g of yellow material. MS (APCI+, 20 V): 409.09 ([M + H], 100%). ^{1}H NMR (400 MHz, $CDCl_3$, δ, ppm): 8.43 (s, 1H, Ar), 8.21 (dd, 3H, J_1 = 7.7, J_2 = 3.7 Hz, Ar), 8.16 (s, 1H, Ar), 7.97 (d, 2H, J = 8.3 Hz, Ar), 7.80 (dd, 1H, J_1 = 8,4, J_2 = 1.6 Hz, Ar), 7.70 (d, 2H, J = 8.3 Hz, Ar), 7.60-7.52 (m, 2H, Ar), 7.50 (d, 1H, J = 3.3 Hz, Ar), 7.47 (d, 1H, J = 7.8 Hz, Ar), 7.38-7.32 (m, 3H, Ar), 7.29 (s, 1H, Ar). ^{13}C NMR (400 MHz, $CDCl_3$, δ, ppm): 141.30, 141.00, 140.02, 139.15, 136.11, 132.08, 128.61, 127.41, 126.24, 126.02, 125.97, 125.37, 124.06, 123.40, 120.45, 120.33, 119.91, 119.77, 118.94, 111.01, 110.83, 109.92.

4.2.3 4,4′-Di(3-phenylcarbazol-9-yl)benzophenone (BPBCzO). 0.5 g (2.06 mmol) of 3-phenyl-9*H*-carbazole (**2**) and 0.16 g (6.67 mmol) of sodium hydride were stirred in 10 ml of DMF at room temperature under nitrogen for 30 min. Then, 0.21 g (0.96 mmol) of 4,4′-difluorobenzophenone was added and the resulting reaction mixture was stirred at 100 °C under nitrogen for 24 h. After TLC control the reaction mixture was cooled and quenched by the addition of ice water. The product was extracted by chloroform. The combined extract was dried over anhydrous Na_2SO_4. The crude product was purified by silica gel column chromatography using the mixture of THF and hexane (vol. ratio 1 : 5) as an eluent. Yield: 0.27 (42%) g of yellow crystals. M.p: 123 °C (DSC). MS (APCI +, 20 V): 664.55 ([M + H], 100%). ^{1}H NMR (400 MHz, $CDCl_3$, δ, ppm): 8.35 (d, 2H, J = 40.3 Hz, Ar), 8.12 (dd, 6H, J_1 = 15.0, J_2 = 9.2 Hz, Ar), 8.06–7.86 (m, 2H, Ar), 7.79–7.59 (m, 8H, Ar), 7.58–7.35 (m, 8H, Ar), 7.28 (dd, 4H, J_1 = 17.6, J_2 = 10.4 Hz, Ar), 7.18 (s, 2H, Ar). ^{13}C NMR (400 MHz, $CDCl_3$, δ, ppm): 193.32, 132.05, 131.96, 131.91, 129.42, 128.93, 128.87, 127.36, 127.01, 126.49, 126.46, 126.39, 125.80, 120.87, 120.72, 120.70, 120.62, 120.54, 119.02, 111.82, 110.08, 109.97, 109.82.

4.2.4 4,4′-Di{3-[4-(carbazol-9-yl)phenyl]carbazol-9-yl}benzophenone (BCzBCzO). 0.6 g (1.47 mmol) of 3-[4-(karbazol-9-yl)phenyl]-9*H*-carbazole (**2**) and 0.11 g (4.58 mmol) of sodium hydride were stirred in 10 ml of DMF at room temperature under nitrogen for 30 min. Then, 0.15 g (0.69 mmol) of 4,4′-difluorobenzophenone was added and the resulting reaction mixture was stirred at 100 °C under nitrogen for 24 h. After TLC control the reaction mixture was cooled and quenched by the addition of ice water. The product was extracted by chloroform. The combined extract was dried over anhydrous Na_2SO_4. The crude product was purified by silica gel column chromatography using the mixture of THF and hexane (vol. ratio 1 : 3) as an eluent. Yield: 0.36 g (54%) of yellow crystals. M.p.: 366 °C (DSC). MS (APCI+, 20 V): 969.46 ([M + H], 100%). ^{1}H NMR (400 MHz, $CDCl_3$, δ, ppm): 8.39 (d, 2H, J = 6.8 Hz, Ar), 8.16 (dd, 6H, J_1 = 11.6 Hz, J_2 = 8.0 Hz, Ar), 8.09 (d, 4H, J = 7.7 Hz, Ar), 7.82 (dd, 8H, J_1 = 36.3 Hz, J_2 = 7.9 Hz, Ar), 7.71 (t, 2H, J = 7.7 Hz, Ar), 7.62-7.56 (m, 6H, Ar), 7.53 (d, 2H, J = 8.2 Hz, Ar), 7.43 (d, 6H, J = 8.1 Hz, Ar), 7.39-7.28 (m, 6H, Ar), 7.23 (t, 4H, J = 7.3 Hz, Ar). ^{13}C NMR (400 MHz, $CDCl_3$, δ, ppm): 194.43, 141.83, 140.96, 140.87, 140.81, 139.93, 136.41, 135.96, 133.31, 132.01, 128.66, 127.49, 126.68, 126.45, 126.00, 125.72, 124.62, 124.00, 123.45, 121.03, 120.67, 120.38, 119.98, 119.09, 110.31, 110.08, 109.90.

4.3. General information

To obtain thermal properties of newly synthesized carbazole-benzophenone derivates, thermo-gravimetric analysis (TGA) and differential scanning calorimetry (DSC) were performed using a TGAQ50 apparatus and Bruker Reflex II thermos-system, respectively. During TGA and DSC measurement, a heating rate of 10 °C min^{-1} in a nitrogen atmosphere was used. To investigate photophysical properties, *i.e.* ultraviolet-visible (UV-vis) absorption, photoluminescence (PL) spectra at 300 K, and photoluminescence (PL) spectra at 77K was measured using Shimadzu UV-2450, PerkinElmer LS55 and Hitachi F-7000 fluorescence spectrophotometer with a delay time of 1 ms instruments. The optical band gap energy was estimated using the first edge wavelength of UV-vis absorption spectra. The excitation wavelength of 350 nm was used to measure PL spectra of these materials at room temperature with a 10 nm minute^{-1} scanning rate. The onset of photoluminescence (PL) spectra measured at 77 K was used to estimate the triplet energies of materials. A computer mounted CH-instruments CH1604A potentiostat was utilized to carry-out electrochemical analysis of these novel materials. The electrochemical system consisted of three electrodes such as a glassy carbon electrode as a working point, a platinum rod as an auxiliary electrode, and a silver/silver chloride rode as the reference electrode. The electrochemical analysis was carried out at room temperature under a nitrogen environment in dichloromethane (DCM) using 0.1 M tetrabutylammonium perchlorate (Bu_4NClO_4) as the auxiliary electrolyte material. The cyclic voltammetry curves were recorded on a computer.

4.4. Device fabrication and characterizations

The studied TADF organic LEDs were fabricated using pre-cleaned ITO-coated glass substrates, having a sheet resistance of 15 Ω cm^{-2}. The green TADF organic LEDs consisted following device configurations: ITO (125 nm)/PEDOT:PSS (35 nm)/Hosts: X wt% **4CzIPN** (20 nm)/PO-T2T (10 nm)/TPBi (30 nm)/LiF (1 nm)/Al (200 nm) and ITO (125 nm)/PEDOT:PSS (35 nm)/VPEC (10 nm)/Hosts: X wt% **4CzIPN** (20 nm)/PO-T2T (10 nm)/TPBi (30 nm)/LiF (1 nm)/Al (200 nm), as shown in Fig. S1 and S2 in ESI,† where PEDOT:PSS acted as the hole-injection layer, VPEC as hole-transport and electron blocking layer, TPBi worked as

the electron transport layer, and LiF and Al acted as an electron-injection and a cathode, respectively. Where we have hosts: **BPBCzO**, and **BCzBCzO**, X signifies the dopant concentrations incorporated to optimize the device conditions. Before device fabrication, ITO-coated glass substrates were cleaned according to the approach previously reported. At first, the aqueous solution of PEDOT:PSS was spin-coated on the precleaned substrates at 4000 rpm for 20 s to form a hole-injection layer and then kept on a hot plate for annealing it up to 30 min at 100 °C. Then 4 mg ml^{-1} VPEC solution was prepared in chlorobenzene and spin-coated on PEDOT:PSS thin-film and kept on a hot plate to anneal it at 130 °C for 20 min. Then, it was followed by the deposition of emissive layer with spin-coating from host: X wt% of **4CzIPN** mixture, which was prepared by dispersing it in *ortho*-xylene solvent. Then after, an electron-transporting layer TPBi, an electron-injection layer LiF, and an Al cathode by thermal evaporation in a chamber having a vacuum level of 4×10^{-6} Torr. After the fabrication of devices, we kept them in a small vacuum chamber and tested them one-by-one. The testing process was performed in the artificial dark room. A computer mounted electrometer (Keithley source measurement unit (CS-2400)) was used to apply current on the device for measuring current–voltage–luminance (*J–V–L*) characteristics. We also used Photo Research PR-655 spectrum scan and CS-100A luminance meter to measure CIE chromatic coordinates, EL spectra, and luminance. All the characterizations were carried-out in artificial dark room. Lifetime of TADF organic LEDs were measured by computer mounted lifetime ageing system.

Conflicts of interest

Author declare that there are no conflicts of interest.

Acknowledgements

The authors are highly thankful for the financial support provided by Ministry of Science and Technology, Taiwan (109-2923-M-007-003-MY3 and 108-2923-M-007-002-MY3) and Research Council of Lithuania (grant No. S-MIP-22-84). Authors are also highly thankful to National Tsing Hua University and Kaunas University of Technology for providing instrument facility for the materials characterization and device fabrication. D. T. is obliged for World Federation of Scientists for support.

References

1 M. Godumala, J. Hwang, H. Kang, J.-E. Jeong, A. K. Harit, M. J. Cho, H. Y. Woo, S. Park and D. H. Choi, High-Performance, Solution-Processable Thermally Activated Delayed Fluorescent Organic Light-Emitting Diodes Realized via the Adjustment of the Composition of the Organoboron Acceptor Monomer in Copolymer Host Materials, *ACS Appl. Mater. Interfaces*, 2020, **12**, 35300–35310.

2 P. S. Ngo, M.-K. Hung, K.-W. Tsai, S. Sharma and S. A. Chen, Highly Efficient Solution-Processed Thermally Activated Delayed Fluorescence Bluish-Green and Hybrid White Organic Light-Emitting Diodes Using Novel Bipolar Host Materials, *ACS Appl. Mater. Interfaces*, 2019, **11**, 45939–45948.

3 Y. Liu, X. Wei, Z. Li, J. Liu, R. Wang, X. Hu, P. Wang, Y. Yamada-Takamura, T. Qi and Y. Wang, Highly Efficient, Solution-Processed Organic Light-Emitting Diodes Based on Thermally Activated Delayed-Fluorescence Emitter with a Mixed Polymer Interlayer, *ACS Appl. Energy Mater.*, 2018, **1**, 543–551.

4 W. Zeng, H. Y. Lai, W. K. Lee, M. Jiao, Y. J. Shiu, C. Zhong, S. Gong, T. Zhou, G. Xie and M. Sarma, Achieving Nearly 30% External Quantum Efficiency for Orange–Red Organic Light Emitting Diodes by Employing Thermally Activated Delayed Fluorescence Emitters Composed of 1,8-Naphthalimide-Acridine Hybrids, *Adv. Mater.*, 2018, **30**, 1704961.

5 Y. Zou, S. Gong, G. Xie and C. Yang, Design Strategy for Solution-Processable Thermally Activated Delayed Fluorescence Emitters and Their Applications in Organic Light-Emitting Diodes, *Adv. Opt. Mater.*, 2018, **6**, 1800568.

6 J.-X. Chen, W.-W. Tao, Y.-F. Xiao, K. Wang, M. Zhang, X.-C. Fan, W.-C. Chen, J. Yu, S. Li and F.-X. Geng, Efficient Orange-Red Thermally Activated Delayed Fluorescence Emitters Feasible for Both Thermal Evaporation and Solution Process, *ACS Appl. Mater. Interfaces*, 2019, **11**, 29086–29093.

7 N. Ikeda, S. Oda, R. Matsumoto, M. Yoshioka, D. Fukushima, K. Yoshiura, N. Yasuda and T. Hatakeyama, Solution-Processable Pure Green Thermally Activated Delayed Fluorescence Emitter Based on the Multiple Resonance Effect, *Adv. Mater.*, 2020, **32**, 2004072.

8 G. Xie, X. Li, D. Chen, Z. Wang, X. Cai, D. Chen, Y. Li, K. Liu, Y. Cao and S. J. Su, Evaporation- and Solution-Process-Feasible Highly Efficient Thianthrene-9,9′,10,10′-Tetraoxide-Based Thermally Activated Delayed Fluorescence Emitters with Reduced Efficiency Roll-Off, *Adv. Mater.*, 2016, **28**, 181–187.

9 Y. J. Cho, B. D. Chin, S. K. Jeon and J. Y. Lee, 20% External Quantum Efficiency in Solution-Processed Blue Thermally Activated Delayed Fluorescent Devices, *Adv. Funct. Mater.*, 2015, **25**, 6786–6792.

10 Y. J. Cho, S. K. Jeon and Y. J. Lee, Molecular Engineering of High Efficiency and Long Lifetime Blue Thermally Activated Delayed Fluorescent Emitters for Vacuum and Solution Processed Organic Light-Emitting Diodes, *Adv. Opt. Mater.*, 2016, **4**, 688–693.

11 J. X. Chen, W. W. Tao, W. C. Chen, Y. F. Xiao, K. Wang, C. Cao, J. Yu, S. Li, F. X. Geng and C. Adachi, Red/Near-Infrared Thermally Activated Delayed Fluorescence OLEDs with Near 100% Internal Quantum Efficiency, *Angew. Chem.*, 2019, **131**, 14802–14807.

12 Q. Zhang, D. Tsang, H. Kuwabara, Y. Hatae, B. Li, T. Takahashi, S. Y. Lee, T. Yasuda and C. Adachi, Nearly 100% Internal Quantum Efficiency in Undoped Electroluminescent Devices Employing Pure Organic Emitters, *Adv. Mater.*, 2015, **27**, 2096–2100.

13 X. Li, J. Zhang, Z. Zhao, L. Wang, H. Yang, Q. Chang, N. Jiang, Z. Liu, Z. Bian and W. Liu, Deep Blue Phosphorescent Organic Light-Emitting Diodes with CIEy Value of 0.11 and External Quantum Efficiency up to 22.5%, *Adv. Mater.*, 2018, **30**, 1705005.

14 B. Zhao, H. Zhang, Y. Miao, Z. Wang, L. Gao, H. Wang, Y. Hao, B. Xu and W. Li, Low Turn-On Voltage and Low Roll-Off Rare Earth Europium Complex-Based Organic Light-Emitting Diodes with Exciplex as the Host, *J. Mater. Chem. C*, 2017, **5**, 12182–12188.

15 G. Lu, Z. G. Wu, R. Wu, X. Cao, L. Zhou, Y. X. Zheng and C. Yang, Semitransparent Circularly Polarized Phosphorescent Organic Light-Emitting Diodes with External Quantum Efficiency over 30% and Dissymmetry Factor Close to 10^{-2}, *Adv. Funct. Mater.*, 2021, **31**, 2102898.

16 X. Yang, G. Zhou and W.-Y. Wong, Functionalization of phosphorescent emitters and their host materials by main-group elements for phosphorescent organic light-emitting devices, *Chem. Soc. Rev.*, 2015, **44**, 8484–8575.

17 X. Yang, B. Jiao, J.-S. Dang, Y. Sun, Y. Wu, G. Zhou and W.-Y. Wong, Achieving High-Performance Solution-Processed Orange OLEDs with the Phosphorescent Cyclometalated Trinuclear Pt(II) Complex, *ACS Appl. Mater. Interfaces*, 2018, **10**, 10227–10235.

18 T. Huang, W. Jiang and L. J. Duan, Recent Progress in Solution Processable TADF Materials for Organic Light-Emitting Diodes, *J. Mater. Chem. C*, 2018, **6**, 5577–5596.

19 Y. Tao, K. Yuan, T. Chen, P. Xu, H. Li, R. Chen, C. Zheng, L. Zhang and W. Huang, Thermally Activated Delayed Fluorescence Materials Towards the Breakthrough of Organoelectronics, *Adv. Mater.*, 2014, **26**, 7931–7958.

20 X.-K. Chen, D. Kim and J.-L. Brédas, Thermally Activated Delayed Fluorescence (TADF) Path toward Efficient Electroluminescence in Purely Organic Materials: Molecular Level Insight, *Acc. Chem. Res.*, 2018, **51**, 2215–2224.

21 C. H. Chen, W. C. Ding, B. Y. Lin, J. J. Huang, M. K. Leung, J. H. Lee and T. L. Chiu, Long-Distance Triplet Diffusion and Well-Packing Hosts with Ultralow Dopant Concentration for Achieving High-Efficiency TADF OLED, *Adv. Opt. Mater.*, 2021, **9**, 2100857.

22 Y. L. Zhang, Q. Ran, Q. Wang, Y. Liu, C. Hänisch, S. Reineke, J. Fan and L. S. Liao, High-Efficiency Red Organic Light-Emitting Diodes with External Quantum Efficiency Close to 30% Based on a Novel Thermally Activated Delayed Fluorescence Emitter, *Adv. Mater.*, 2019, **31**, 1902368.

23 J. Lee, N. Aizawa, M. Numata, C. Adachi and T. Yasuda, Versatile Molecular Functionalization for Inhibiting Concentration Quenching of Thermally Activated Delayed Fluorescence, *Adv. Mater.*, 2017, **29**, 1604856.

24 M. Hasan, S. Saggar, A. Shukla, F. Bencheikh, J. Sobus, S. K. McGregor, C. Adachi, S.-C. Lo and E. B. Namdas, Probing Polaron-Induced Exciton Quenching in TADF Based Organic Light-Emitting Diodes, *Nat. Commun.*, 2022, **13**, 1–7.

25 M. Hasan, A. Shukla, V. Ahmad, J. Sobus, F. Bencheikh, S. K. McGregor, M. Mamada, C. Adachi, S. C. Lo and E. B. Namdas, Exciton–Exciton Annihilation in Thermally Activated Delayed Fluorescence Emitter, *Adv. Funct. Mater.*, 2020, **30**, 2000580.

26 X. Wu, B.-K. Su, D.-G. Chen, D. Liu, C. C. Wu, Z.-X. Huang, T.-C. Lin, C.-H. Wu, M. Zhu and E. Y. Li, The Role of Host–Guest Interactions in Organic Emitters Employing MR-TADF, *Nat. Photonics*, 2021, **15**, 780–786.

27 Q. Wang, Y.-X. Zhang, Y. Yuan, Y. Hu, Q.-S. Tian, Z.-Q. Jiang and L.-S. Liao, Alleviating Efficiency Roll-Off of Hybrid Single-Emitting Layer WOLED Utilizing Bipolar TADF Material as Host and Emitter, *ACS Appl. Mater. Interfaces*, 2018, **11**, 2197–2204.

28 X. Liu, C.-Y. Chan, F. Mathevet, M. Mamada, Y. Tsuchiya, Y.-T. Lee, H. Nakanotani, S. Kobayashi, M. Shiochi and C. Adachi, Isotope Effect of Host Material on Device Stability of Thermally Activated Delayed Fluorescence Organic Light-Emitting Diodes, *Small Sci.*, 2021, **1**, 2000057.

29 N. R. Wallwork, M. Mamada, A. Shukla, S. K. McGregor, C. Adachi, E. B. Namdas and S.-C. Lo, High-Performance Solution-Processed Red Hyperfluorescent OLEDs Based on Cibalackrot, *J. Mater. Chem. C*, 2022, **10**, 4767–4774.

30 L. Shihao, Z. Letian and X. Wenfa, Solution Processed Organic Light-Emitting Devices: Structure, Device Physics and Fabrication Process, *Opto-Electron. Eng.*, 2022, **49**(5), 210407–210413.

31 M. I. Alam, M. R. Nagar, S. R. Nayak, A. Choudhury, J. H. Jou and S. Vaidyanathan, Acceptor Interlocked Molecular Design for Solution-Processed Stable Deep-Blue TADF and Hyper Fluorescence Organic LED Enabling High-Efficiency, *Adv. Opt. Mater.*, 2022, **10**, 2200376.

32 Z. Xie, C. Cao, Y. Zou, X. Cao, C. Zhou, J. He, C. S. Lee and C. Yang, Molecular Engineering Enables TADF Emitters Well Suitable for Non-Doped OLEDs with External Quantum Efficiency of Nearly 30%, *Adv. Funct. Mater.*, 2022, **32**, 2112881.

33 T. Hua, J. Miao, H. Xia, Z. Huang, X. Cao, N. Li and C. Yang, Sulfone-Incorporated Multi-Resonance TADF Emitter for High-Performance Narrowband Blue OLEDs with EQE of 32%, *Adv. Funct. Mater.*, 2022, 2201032.

34 A. Kumar, W. Lee, T. Lee, J. Jung, S. Yoo and M. H. Lee, Triarylboron-Based TADF Emitters With Perfluoro Substituents: High-Efficiency OLEDs With a Power Efficiency Over 100 l m W^{-1}, *J. Mater. Chem. C*, 2020, **8**, 4253–4263.

35 G. Kreiza, D. Berenis, D. Banevičius, S. Juršėnas, T. Javorskis, E. Orentas and K. Kazlauskas, High Efficiency and Extremely Low Roll-Off Solution- and Vacuum-Processed OLEDs Based on Isophthalonitrile Blue TADF Emitter, *Chem. Eng. J.*, 2021, **412**, 128574.

36 Y. Suzuki, Q. Zhang and C. Adachi, A Solution-Processable Host Material of 1,3-bis{3-[3-(9-Carbazolyl)phenyl]-9-carbazolyl}benzene and its Application in Organic Light-Emitting Diodes Employing Thermally Activated Delayed Fluorescence, *J. Mater. Chem. C*, 2015, **3**, 1700–1706.

37 C. Y. Kim, C. Lee, H. J. Kim, J. Hwang, M. Godumala, J.-E. Jeong, H. Y. Woo, M. J. Cho, S. Park and D. H. Choi, Achievement of High Efficiency with Extremely Low

Efficiency Roll-Off in Solution-Processed Thermally Activated Delayed Fluorescence OLEDs Manufactured Using Xanthone-Based Bipolar Host Materials, *J. Mater. Chem. C*, 2020, **8**, 6780–6787.

38 L.-Y. Zhao, Y.-N. Liu, S.-F. Wang, Y.-T. Tao, F.-F. Wang, X.-W. Zhang and W. Huang, Novel Hyperbranched Polymers as Host Materials For Green Thermally Activated Delayed Fluorescence OLEDs, *Chin. J. Polym. Sci.*, 2017, **35**, 490–502.

39 S. Shao, S. Wang, X. Xu, Y. Yang, J. Lv, J. Ding, L. Wang, X. Jing and F. Wang, Bipolar Poly(arylene phosphine oxide) Hosts with Widely Tunable Triplet Energy Levels for High-Efficiency Blue, Green, and Red Thermally Activated Delayed Fluorescence Polymer Light-Emitting Diodes, *Macromolecules*, 2019, **52**, 3394–3403.

40 S. H. Tucker, Iodination in the Carbazole Series, *J. Chem. Soc.*, 1926, **129**, 546–553.

41 J. W. Sun, J. H. Lee, C. K. Moon, K. H. Kim, H. Shin and J. J. Kim, A Fluorescent Organic Light-Emitting Diode with 30% External Quantum Efficiency, *Adv. Mater.*, 2014, **26**, 5684–5688.

42 D. R. Lee, B. S. Kim, C. W. Lee, Y. Im, K. S. Yook, S.-H. Hwang and J. Y. Lee, Above 30% External Quantum Efficiency in Green Delayed Fluorescent Organic Light-Emitting Diodes, *ACS Appl. Mater. Interfaces*, 2015, **7**, 9625–9629.

43 J.-H. Jou, T.-H. Li, S. Kumar, C.-C. An, A. Agrawal, S.-Z. Chen, P.-H. Fang, G. Krucaite, S. Grigalevicius and J. Grazulevicius, Enabling High-Efficiency Organic Light-Emitting Diodes with a Cross-Linkable Electron Confining Hole Transporting Material, *Org. Electron.*, 2015, **24**, 254–262.

44 S. G. Ihn, N. Lee, S. O. Jeon, M. Sim, H. Kang, Y. Jung, D. H. Huh, Y. M. Son, S. Y. Lee and M. Numata, An Alternative Host Material for Long-Lifespan Blue Organic Light-Emitting Diodes Using Thermally Activated Delayed Fluorescence, *Adv. Sci.*, 2017, **4**, 1600502.

45 S. K. Jeon, H.-J. Park and J. Y. Lee, Blue-Shifted Emission Color and High Quantum Efficiency in Solution-Processed Blue Thermally Activated Delayed Fluorescence Organic Light-Emitting Diodes Using an Intermolecular Interaction Suppressing Host Decorated with Blocking Groups, *J. Mater. Chem. C*, 2018, **6**, 6778–6783.

